An *ex situ* study of the adsorption of calcium phosphate from solution onto TiO_2(110) and Al_2O_3(0001)

M. Murphy[1], M.S. Walczak[1], H. Hussain[1], M.J. Acres[1], C.A. Muryn[2], A.G. Thomas[3], N. Silikas[4], and R. Lindsay[1]

[1]*Corrosion and Protection Centre, School of Materials, The University of Manchester, Sackville Street, Manchester, M13 9PL, UK*

[2]*Chemistry and Photon Science Institute, Alan Turing Building, The University of Manchester, Oxford Road, Manchester, M13 9PL, UK*

[3]*School of Materials and Photon Science Institute, The University of Manchester, Manchester, M13 9PL, UK*

[4]*Biomaterials Unit, School of Dentistry, The University of Manchester, Manchester, M13 9PL, UK*

Corresponding Author:

Robert Lindsay

Tel: +44 161 306 4824

Fax: +44 161 306 4865

Email: robert.lindsay@manchester.ac.uk

Abstract

Ex situ atomic force microscopy and x-ray photoelectron spectroscopy are employed to characterise the adsorption of calcium phosphate from an aqueous solution of $CaCl_2.H_2O$ and KH_2PO_4 onto rutile-TiO_2(110) and α-Al_2O_3(0001). Prior to immersion, the substrates underwent *wet chemical* preparation to produce well-defined surfaces. Calcium phosphate adsorption is observed on both rutile-TiO_2(110) and α-Al_2O_3(0001), with atomic force microscopy images indicating island-type growth. In contrast to other studies on less well-defined TiO_2 and Al_2O_3 substrates, the induction period for calcium phosphate nucleation appears to be comparable on these two surfaces.

Keywords: metal oxide; low miller index single crystal surface; aqueous solution; deposition; surface composition; film growth

1.0 Introduction

During Richard Lambert's tenure as an editor of Surface Science, mechanistic insight into surface properties has developed enormously. Progress has been facilitated by the application of new advanced probes, along with tremendous improvements in the predictive power of theoretical modelling. Research effort has also moved away from concentrating on relatively simple *model* surface systems to those that are both more challenging and technologically pertinent. For example, when Richard took up his editorship in 1993, the study of metal oxide surfaces was a niche activity. In the intervening 20, or so, years, this subject has emerged as one of the established themes of surface science [1,2]. Many important topics have been examined, including defect phenomena [3], surface polarity [4], and wet interfaces [5]. In this paper, we contribute to the latter area through examining the adsorption of calcium phosphate from aqueous solution onto rutile-TiO_2(110) and α-Al_2O_3(0001).

To a significant extent, interest in calcium phosphate/metal oxide interfaces is generated by their relevance to the performance of implant materials, including osseointegration (i.e. bonding with bone) [6]; metal oxide, rather than metallic, substrates are of concern as they are more likely to be characteristic of an *in situ* implant surface termination, and calcium phosphate represents the inorganic component of bone. Specific motivation for the current study is derived from reports that in aqueous solution the nucleation of calcium phosphate on TiO_2 is more rapid than on some other metal oxide substrates, which suggests that the surface chemistry of TiO_2 enhances the kinetics of this process. For example, Song *et al* found that calcium phosphate nucleation occurred more rapidly on TiO_2 powders than those composed of either Al_2O_3 or SiO_2 [7]. Other data acquired from thin films of TiO_2 and Al_2O_3 are consistent with this result [8].

One concern about the conclusion that the surface chemistry of TiO_2 in some way promotes nucleation of calcium phosphate from the aqueous phase is that studies performed to date have been undertaken on somewhat ill-defined substrates (i.e. powders, thin films [7,8]). On this basis, it may be proposed that surface morphology rather than chemistry dominates calcium phosphate nucleation kinetics. Here, we test this possibility through studying the adsorption of calcium phosphate from aqueous solution onto two well-defined single crystal metal oxide surfaces, i.e. rutile-TiO_2(110) and α-Al_2O_3(0001). Primarily, *ex situ* atomic force microscopy (AFM) and X-ray photoelectron spectroscopy (XPS) were applied to characterise the resulting interfaces. Low energy electron diffraction (LEED) was also undertaken to assess long-range surface order.

2.0 Materials and methods

Experimental work was undertaken with single crystal samples of rutile-TiO_2(110) and α-Al_2O_3(0001) purchased from PI-KEM. Prior to studying calcium phosphate adsorption, samples underwent cleaning in order to produce well-defined surfaces, i.e. large flat terraces separated by monatomic steps. For this purpose a *wet chemical* recipe was applied, which has previously proven suitable for such preparation of rutile-TiO_2(110) [9]. Briefly, this approach consists of 4 steps, beginning with sonication of the sample in a sequence of solvents (i.e. acetone, ethanol, and deionised water), and drying in a stream of nitrogen. The second step involves annealing the sample in air in a tube furnace for between 60 min and 90 min; anneal temperatures of 973 K and 1373 K were employed for rutile-TiO_2(110) and α-Al_2O_3(0001), respectively. Following cooling, the sample is immersed in aqua regia (a 3:1 by volume mixture of concentrated HCl and HNO_3) at room temperature for ~ 45 min, and then rinsed thoroughly with deionised water. Finally, the sample is inserted into a UV-ozone cleaner

(Novascan), where it is initially exposed to UV-light, and then left immersed in the locally generated ozone atmosphere.

A number of rutile-TiO_2(110) and α-Al_2O_3(0001) samples were prepared, as outlined above, to enable the temporal evolution of calcium phosphate adsorption following submersion in aqueous solution to be studied. Regarding details of this solution, it was prepared by combining 20 mL of 7 mM $CaCl_2.2H_2O$ (≥ 99.0% Sigma Aldrich) with 20 mL of 7.6 mM KH_2PO_4 (≥ 99.0% Sigma Aldrich), using deionised water as the solvent. Prior to mixing, the pH of each solution was adjusted to 6.5 through addition of ~ 1 M NaOH solution (≥ 99.0% Sigma Aldrich). The resulting solution is similar to that employed in Ref. 8, containing 3.5 mM of Ca^{2+} and 3.8 mM of $H_2PO_4^-$/HPO_4^{2-}/PO_4^{3-}. Henceforth, this aqueous solution will be referred to as *CP solution*. Substrate immersion in the *CP solution* was undertaken in glass beakers containing ~ 40 mL of the solution at ~ 295 K. Upon removal of a sample from solution, it was immediately thoroughly rinsed with deionised water to avoid evaporation and subsequent physical deposition of solution components onto the sample surface

Concerning surface characterization, AFM images were acquired both from as-prepared samples (i.e. not subjected to immersion in *CP solution*), as well from those that had been submerged for periods of 1 h, 2 h, or 3 h. Imaging was undertaken in air at room temperature with a Multimode 8 AFM (Bruker) in Peak Force Tapping mode. To obtain LEED patterns, samples were inserted through a load-lock into an appropriately equipped ultra high vacuum (UHV) chamber. A 4-grid rear view LEED optics (Omicron) was employed to collect the data. Sample charging was an issue during acquisition of LEED patterns, due to the insulating nature of the wet chemically prepared samples.

XPS measurements were performed with either a Kratos Axis Ultra system or a SPECS XPS instrument, which is also capable of measurements at near ambient pressure (not utilised here). Both facilities were equipped with a load lock system for sample introduction, and monochromated Al Kα X-rays ($h\nu$ = 1486.6 eV, $\Delta h\nu \sim 0.6$ eV) were employed in both instances as the photon source. Emitted photoelectrons were collected using either a 165 mm hemispherical energy analyser (Kratos), or a 150 mm hemispherical energy analyser (Phoibos 150, SPECS). To increase the surface sensitivity of the spectra a photoelectron emission angle (θ_E) of 50° was employed for the majority of the measurements (θ_E = 0° is emission along the surface normal). Charge accumulation during data collection was compensated by exposing samples to a flood of low energy electrons. Binding energies (BEs) were calibrated by assigning a BE value of 285.0 eV to the C 1s hydrocarbon component of adsorbed adventitious carbon [10].

Fitting of XPS profiles was undertaken with CasaXPS software [11]. Gaussian-Lorentzian (GL) line shape functions (30% Lorentzian) were employed to model all of the photoelectron peaks. Inelastically scattered background electrons were described with a Shirley-type function [12].

3.0 Results and Discussion

Before discussing the evolution of the submerged substrates, we demonstrate the utility of the *wet chemical* recipe for preparing both rutile-TiO_2(110) and α-Al_2O_3(0001). Fig. 1 shows typical LEED and AFM data acquired from as-prepared surfaces. Focusing initially upon the results obtained for rutile-TiO_2(110), the LEED (Fig. 1(a)) and AFM (Fig. 1(b) and (c)) data are consistent with those presented previously to illustrate the potential of the *wet chemical* approach [9]. More specifically, a sharp (1x1) rectangular LEED pattern is observed (Fig. 1(a)), suggesting significant translational surface order. In agreement with this conclusion, the AFM image (Fig 1. (b)) and associated line profile (Fig. 1 (c)) provide direct evidence that

the surface consists of relatively large, flat terraces, separated by well-defined steps; the most typical measured step height (~ 0.3 nm) is consistent with the value expected for a monatomic step (0.33 nm) on rutile-TiO_2(110) [13].

Turning to the as-prepared α-Al_2O_3(0001) surface, the LEED pattern (Fig. 1(d)) displays a sharpness similar to Fig. 1(a), and is consistent with the threefold symmetry expected for this surface [14,15]. The relative dimensions of the reciprocal surface unit cell are consistent with an unreconstructed (1x1) surface. Moreover, the AFM image (Fig. 1 (e)) and line profile (Fig. 1(f)) again show that the surface is comprised of relatively large, flat terraces separated by monoatomic steps; the expected monatomic step height on this surface is 0.22 nm [15], which compares well with the typically measured height of ~ 0.2 nm.

Concerning the composition of the as-prepared surfaces, XPS data are displayed in Fig. 2. An overview XPS spectrum of TiO_2(110) is displayed in Fig.2 (a). Intense peaks arising from Ti and O core levels are clearly discernable (see figure for labelling). In addition, there is a significant C 1s feature, which we attribute to surface adsorbed adventitious carbon [10]. It should be noted that in Ref. 9, it was demonstrated that UV-ozone treatment could remove this carbon layer. Here, such cleanliness was neither achieved nor indeed particularly pursued, as samples were to be subsequently immersed in aqueous solution. Other smaller peaks were also sometimes visible in TiO_2(110) overview XPS spectra, including core level signals due to silicon and nitrogen (e.g. N 1s feature is labelled in Fig. 2 (a)). It is concluded that these species are either bulk contaminants or a result of minor surface contamination arising from the *wet chemical* preparation.

Higher resolution Ti 2p and O 1s core level XPS spectra acquired from the as-prepared TiO_2(110) surface, along with best-fits to the profiles, are displayed in Figs. 2 (b) and (c),

respectively. Focussing initially upon the Ti 2p data, the most intense feature (BE ~ 458.9 eV) can be assigned to the Ti $2p_{3/2}$ spin-orbit component of Ti cations in the +4 oxidation state, as expected for TiO_2 [16]. The displayed best-fit, which assumes only a contribution from Ti^{4+}, is evidently of high quality; a requirement to include a satellite feature (labelled *Sat.*) has been established previously [17]. However, as indicated on the plot (see, also, inset), there is some residual intensity at BE ~ 457.3 eV, which almost certainly arises from a small concentration of Ti cations in the +3 oxidation state [18]. On this basis, it can be concluded that the adopted *wet chemical* preparation appears to result in a near stoichiometric TiO_2(110) surface. Regarding the O 1s core level XPS spectrum in Fig. 2 (c), four G-L line shape functions (each having a full width at half maximum (fwhm) of ~ 1.1 eV) were required to obtain an acceptable fit to the experimental data. The feature at BE ~ 530.1 eV (labelled O^{2-}) is attributed to signal from substrate oxygen atoms [16,19]. On the basis of measurements undertaken on TiO_2(110) prepared in UHV, the peak at E_B ~ 531.2 eV is most likely to arise from surface bound hydroxyls (OH) [19]. The two higher BE components, which are labelled O^1 (E_B ~ 532.0 eV) and O^2 (E_B ~ 533.0 eV), are suggested to be due to the presence of RC_xO_y components in the adventitious carbon layer [10].

Figs. 2 (d) – (f) display analogous spectra to those in Figs. 2 (a) – (c), but for as-prepared Al_2O_3(0001). Al and O related core level peaks are apparent in the overview spectrum (Fig 2 (d)), along with a C 1s feature, which we again conclude arises from a surface layer of adventitious carbon. The higher resolution Al 2p spectrum (Fig. 2 (e)) has a maximum at BE ~ 74.2 eV, as expected for Al_2O_3 [20], and is fitted with a single spin-orbit split doublet. Five G-L line shape functions (each having a fwhm of ~ 1.3 eV) were required to fit the O 1s core level XPS spectrum (Fig 2. (f)). The most intense component at BE ~ 531.2 eV (labelled O^{2-}) is ascribed to substrate oxygen atoms, and that labelled OH (BE ~ 532.6 eV) to surface bound hydroxyls [20-23]. In agreement with the assignments made for the TiO_2(110) O 1s spectrum

(Fig. 2 (c)), the peaks at BE ~ 531.9 eV (labelled O^1) and BE ~ 533.1 eV (labelled O^2) are concluded to arise from the adventitious carbon layer. The origin of the least intense fifth component, labelled O^3 (BE ~ 529.3 eV) is uncertain; we note that this feature is also apparent in O 1s spectra acquired from $Al_2O_3(0001)$ in Ref. 23**,** although not explicitly discussed.

Regarding the surface layer of adventitious carbon found on both as-prepared substrates, it is estimated to have a thickness of ~ 1.8 nm and ~ 1.4 nm for $TiO_2(110)$ and $Al_2O_3(0001)$, respectively. These values have been calculated, using the approach outlined in Ref. 10, from the relative intensities of the C 1s and Ti 2p (or Al 2p) signals at both $\theta_E = 0°$ and $\theta_E = 50°$. We note that for this calculation it was assumed that the surface region consists of two layers, i.e. adventitious carbon atop the oxide substrate. Clearly, these thickness values indicate that both as-prepared substrates are covered by a number of monolayers of adventitious carbon, which may be of importance as regards surface properties.

Moving to calcium phosphate adsorption, Fig. 3 shows AFM images acquired from $TiO_2(110)$ and $Al_2O_3(0001)$ following immersion for periods in *CP solution* of 1 h, 2 h, and 3h; the AFM images from as-prepared surfaces (0 h) are also shown for comparison. For both substrates, additional discrete protrusions are observed after 1 h of immersion, i.e. material has apparently been deposited from solution. In both of the 1 h images, the amount of surface adsorbed material is such that the underlying terrace-step structure of the substrate remains clearly visible. Subsequent to immersion for 2 h, the quantity of adsorbed material has apparently increased substantially, and substrate steps are barely discernible. After being submerged in solution for 3 h, the adsorbed layers have developed to such an extent that the single crystal substrates are entirely masked. Assuming that the deposited material is indeed calcium phosphate (see XPS data presented below), these images suggest that under the

conditions of this study, the nucleation of calcium phosphate from aqueous solution onto both TiO_2(110) and Al_2O_3(0001) exhibits comparable kinetics.

As to the growth mode of the calcium phosphate on the two substrates, the images in Fig. 3 suggest island type growth. Measurements of protrusion dimensions support this conclusion, as a distribution of heights is found. For example, the apparent heights of islands on both TiO_2(110) and Al_2O_3(0001) after 1 h of immersion range from ~ 0.5 nm to ~ 2 nm; these islands also display a range of apparent widths up to ~ 40 nm, with the mean being approximately 30 nm and 20 nm for TiO_2(110) and Al_2O_3(0001), respectively. A narrower spread of heights would be expected for layer-by-layer type growth. We note that we cannot distinguish between Volmer-Weber and Stranski-Krastanov island-type growth modes from our AFM measurements. However, we have attempted to gain evidence for deposition induced interface ordering through acquiring LEED data from substrates after 1 h of immersion. On the basis of UHV studies indicating that calcium can form ordered overlayers on both TiO_2(110) [24] and Al_2O_3(0001) [14], we hypothesised that similarly ordered overlayers could perhaps exist between the discrete protrusions (islands), but only (1x1) patterns were observed.

One striking difference between calcium phosphate adsorption on TiO_2(110) and Al_2O_3(0001) is apparent in the 1 h immersion images, i.e. there is seemingly a much stronger preference for adsorption at steps on Al_2O_3(0001). This step-edge decoration is revealed by comparing the 0 h (as-prepared) and 1 h images for Al_2O_3(0001), where the latter exhibits a much brighter appearance at steps. The existence of adsorbed material at this location is confirmed in Fig. 4, which displays step-edge line-profiles extracted from the 0 h and 1 h Al_2O_3(0001) images. A clear protrusion (~ 0.8 nm in height) is observed at the step-edge for the 1 h immersed substrate. Considering the origin of this difference in calcium phosphate growth on TiO_2(110) and Al_2O_3(0001), we may speculate that it is likely a result of differences in the

relative reactivity of the steps/terraces; a more definitive answer would require further investigation, including gaining detailed knowledge of the surface structures.

Another observation of possible significance can be derived from comparing the AFM images of the two substrates after 2h and 3 h of immersion. From this assessment, it is evident that the protrusions appear larger on TiO_2(110) than on Al_2O_3(0001) after 2h, but vice versa after 3 h. This phenomenon may suggest some differences in the growth of calcium phosphate on the two substrates. However, in our opinion, the variation in protrusion size is more likely to be simply a result of changes in AFM tip-surface interaction.

To verify that the surface adsorbed material observed in AFM is most likely calcium phosphate, XPS spectra have been acquired from substrates following immersion in CP *solution* for 3h. In Fig. 5 (a) such an overview spectrum of TiO_2(110) is compared to that acquired from the as-prepared surface (0 h). It is evident that immersion gives rise to Ca and P core level signals (2s and 2p), suggesting that the protrusions in AFM images are composed of calcium phosphate. We point out that along with the signals for Ca and P in Fig. 5 (a), there are also features arising from Si (2s and 2p core levels), which, as indicated above, are either due to bulk contaminants or a result of minor surface contamination arising from the *wet chemical* preparation. Comparable overview spectra acquired from Al_2O_3(0001) are displayed in Fig. 5 (d), i.e. data from as-prepared surface (0 h) and 3 h immersed surface. Again, there is clear evidence of surface Ca and P species through the appearance of 2s and 2p core level peaks, i.e. protrusions in AFM are probably composed of calcium phosphate.

To gain insight into the chemical nature of the substrate bound Ca and P species, higher resolution spectra have been acquired of the Ca 2p and P 2p core levels. These data are displayed in Figure 5 (b) and (c), and (e) and (f) for TiO_2(110) and Al_2O_3(0001), respectively.

In all four spectra, a single spin-orbit split doublet was sufficient to mimic the experimental data. The BEs of the $2p_{3/2}$ components are listed in Table I. Given published XPS data of various calcium phosphate phases [25], it is concluded that these values are consistent with those expected for calcium phosphate; we note that in Ref. 25 BEs were calibrated by assigning a BE value of 284.7 eV to the C 1s hydrocarbon component, rather than the value of 285.0 eV employed in this work. Here, we make no attempt to identify a particular calcium phosphate phase on the basis of either the exhibited BEs or the Ca:P ratio; the latter parameter has been suggested to be not particularly reliable for calcium phoshpate phase determination in Ref. 25.

In addition to calcium phosphate adsorption leading to the emergence of Ca 2p and P 2p core level features, it may be expected that the O 1s spectrum should also reflect the presence of calcium phosphate. According to Ref. 25, an O 1s peak associated with calcium phosphate should appear at BEs ranging from ~ 530.9 to ~ 531.6 eV. Figure 6 (a) and (b) compare the O 1s XPS spectra acquired from as-prepared and 3 h immersed TiO_2(110) and Al_2O_3(0001), respectively. For the former substrate, there is a substantive change in the spectrum after immersion for 3 h, as indicated by the arrow. However, the origin of this change is unclear, as it may simply result from variation in the adventitious carbon layer. For Al_2O_3(0001), the two spectra in Fig. 6 (b) have very similar profiles. Hence, we conclude that the O1s XPS core level cannot be used to identify the presence of calcium phosphate under the conditions of this study. We also acquired substrate metal 2p core levels (i.e. Ti 2p and Al 2p), and found them to exhibit identical shapes to those from the as-prepared surfaces.

Having demonstrated that, under the current experimental conditions, the induction period for calcium phosphate nucleation onto either TiO_2(110) or Al_2O_3(0001) is similar, it is important to compare this result with the previous reports of much faster nucleation kinetics for TiO_2

[7,8]. Given that this earlier work was conducted on less well-defined substrates, our current findings are consistent with the initial hypothesis that surface morphology rather than chemistry dominates calcium phosphate nucleation kinetics. It should, however, be remembered that XPS data indicate that both as-prepared surfaces in the current study are covered by a number of monolayers of adventitious carbon. On this basis, it could be argued that the surface chemistry of the underlying oxide becomes irrelevant here as it is submerged beneath the adventitious carbon, and so it is not surprising that both substrates display similar induction kinetics. However, it is almost certain that the oxide powders studied in Ref. 7 were also initially terminated by adventitious carbon, indicating that this surface layer is unlikely to be the key factor in determining the induction period for calcium phosphate nucleation; we note that in Ref. 8 it is explicitly stated that the TiO_2 thin film surfaces employed in that work were carbon free, but that no such statement is provided for the thin films of Al_2O_3.

Further evidence that calcium phosphate adsorption observed in this study is not simply governed by surface adventitious carbon stems from the AFM images in Fig. 3. As discussed above, they demonstrate a much stronger preference for initial calcium phosphate adsorption at steps on $Al_2O_3(0001)$ than on $TiO_2(110)$. This result illustrates that the identity of the oxide surface does influence aspects of calcium phosphate adsorption. It should be pointed out that it is not even certain that the adventitious carbon layer persists in solution. It may very well be that it dissolves upon immersion only reforming once the sample is removed from the solution.

4.0 Conclusions

In summary, the adsorption of calcium phosphate from aqueous solution onto *wet chemically* prepared rutile-TiO_2(110) and α-Al_2O_3(0001) has been explored, using *ex situ* AFM and XPS. Island-type growth of calcium phosphate is identified on both substrates, with calcium phosphate appearing to display a much stronger preference for decorating step-edges on α-Al_2O_3(0001). Most notably, and in contrast to other studies on less well-defined TiO_2 and Al_2O_3 substrates [7,8], the induction period for calcium phosphate nucleation appears to be similar on rutile-TiO_2(110) and α-Al_2O_3(0001). This result suggests that the conclusion drawn from previous work that the surface chemistry of TiO_2 in some way accelerates nucleation of calcium phosphate is questionable, at least under the conditions of this study.

Acknowledgements

MM acknowledges financial support from EPSRC (EP/G036950/1) through the Advanced Metallic Systems Centre for Doctoral Training. MSW thanks AkzoNobel for funding her postdoctoral research associate position. HH and MA both acknowledge BP for providing funds through a BP-ICAM project.

Table I BEs of the $2p_{3/2}$ component of the Ca 2p and P 2p XPS core level spectra displayed in Figure 5. Data were acquired from rutile-TiO_2(110) and α-Al_2O_3(0001) substrate after immersion for 3 h in *CP solution*.

	Binding Energy (eV)	
	TiO_2(110)	Al_2O_3(0001)
Ca $2p_{3/2}$	347.4	347.7
P $2p_{3/2}$	133.3	133.6

References

1. U. Diebold, S.-C. Li, M. Schmid, Annu. Rev. Phys. Chem. 61 (2010) 129.
2. C.T. Campbell, J. Sauer, Chem. Rev. 113 (2013) 3859.
3. G. Pacchioni, H.-J. Freund, Chem. Rev. 113 (2013) 4035.
4. J. Goniakowski, F. Finocchi, C. Noguera, Rep. Prog. Phys. 71 (2008) 016501.
5. G.E. Brown Jr., G. Calas, Geochemical Perspectives, 1 (2012) 483.
6. L. Le Guéhennec, A. Soueidan, P. Layrolle, Y. Amouriq, Dent. Mater. 23 (2007) 844.
7. L. Song, A.A. Campbell, X.S. Li, B.C. Bunker, Mat. Rec. Soc. Symp. Proc. 414 (1996), 35.
8. M.G. Nooney, A. Campbell, T.S. Murrell, X.-F. Lin, L.R. Hossner, C.C. Chusnei, D.W. Goodman, Langmuir 14 (1998) 2750.
9. M.H.M Ahmed, F.P. Lydiatt, D. Chekulaev, P.L. Wincott, D.J. Vaughan, J.H. Jang, S. Baldelli, A.G. Thomas, W.S. Walters, R. Lindsay, Surf. Sci. 630 (2014) 41.
10. A.A. Al-Refaie, J. Walton, R. A. Cottis, R. Lindsay, Corros. Sci. 52 (2010) 422.
11. Casa Software Ltd, Teignmouth, Devon, UK. http://www.casaxps.com
12. D.A Shirley, Phys. Rev. B, 5 (1972) 4709.
13. H. Takahashi, R. Watanabe, Y. Miyauchi, G. Mizutani, J. Chem. Phys. 134 (2011) 154704.
14. M. Gautier, G. Renaud, L.P. Van, B. Villette, M. Pollak, N. Thromat, F. Jollet, J.-P. Duraud, J. Am. Ceram. Soc. 77 (1994) 323.
15. E.A. Soares, M.A. Van Hove, C.F. Walters, K.F. McCarty, Phys Rev B 65 (2002) 195405.
16. U. Diebold, T.E. Madey, Surf. Sci. Spectra 4 (1996) 227.
17. M. Oku, H. Matsuta, K. Wagatsuma, Y. Waseda, S. Kohiki, J. Electron Spectrosc. 105 (1999) 211.

18. J.-M. Pan, B.L. Maschhoff, U. Diebold, T.E. Madey, J. Vac. Sci. Technol. A 10 (1992) 2470.

19. L.E. Walle, A. Borg, P. Uvdal, A. Sandell, Phys. Rev. B 80 (2009) 235436.

20. J.A. Rotole, P.M.A. Sherwood, Surf. Sci. Spectra 5 (1998) 11.

21. S.A. Chambers, T. Droubay, D.R. Jennison, T.R. Mattsson, Science 297 (2002) 827.

22. Q. Fu, T. Wagner, M. Rühle, Surf. Sci. 600 (2006) 4870.

23. D. Yang, M. Krasowska, R. Sedev, J. Ralston, Phys. Chem. Chem. Phys. 12 (2010) 13724.

24. O. Bikondoa, C.L. Pang, C.A. Muryn, B.G. Daniels, S. Ferrero, E. Michelangeli, G. Thornton, J. Phys. Chem. B 108 (2004) 16768.

25. C.C. Chusuei, D.W. Goodman, M.J. Van Stipdonk, D.R. Justes, E.A. Schweikert, Anal. Chem. 71 (1999) 149.

Figure Captions

Figure 1 **(**a) LEED pattern (beam energy ~ 100 eV), and (b) AFM image of rutile-TiO_2(110) acquired subsequent to *wet chemical* preparation. (c) displays the line profile from along the line indicated in (b). Equivalent LEED (beam energy ~ 110 eV) and AFM data for α-Al_2O_3(0001) are shown in (d), (e), and (f). Surface unit cells are indicated on the LEED patterns.

Figure 2 (a) Overview XPS spectrum, (b) Ti 2p (inset magnifies Ti^{3+} binding energy region) and (c) O 1s core level XPS spectra of rutile-TiO_2(110) acquired subsequent to *wet chemical* preparation ($h\nu$ = 1486.6 eV, θ_E = 50°). (d) Overview XPS spectrum, (e) Al 2p and (f) O 1s core level XPS spectra of α-Al_2O_3(0001) acquired subsequent to *wet chemical* preparation ($h\nu$ = 1486.6 eV, θ_E = 50°). For (b), (c), (e), and (f) best fits (light blue markers) to the experimental data (solid black lines) are also shown, achieved with GL (red lines), and Shirley-type (broken grey lines) functions. Peak assignments, as discussed in the text, are indicated.

Figure 3 AFM images acquired from rutile-TiO_2(110) (top row) and α-Al_2O_3(0001) (bottom row) following immersion in *CP solution* for periods of 1 h, 2 h, and 3h. The AFM images from as-prepared surfaces (0 h) are also shown for comparison. All images have dimensions of 1 μm x 1μm.

Figure 4 Line-profiles over step-edges extracted from the 0 h and 1 h α-Al_2O_3(0001) AFM images displayed in Figure 3.

Figure 5 (a) Overview XPS spectrum, (b) Ca 2p and (c) P 2p core level XPS spectra of rutile-TiO_2(110) acquired subsequent to immersion in *CP solution* for 3 h ($h\nu$ = 1486.6 eV, θ_E = 50°). (d) Overview XPS spectrum, (e) Ca 2p and (f) P 2p core level XPS spectra of α-Al_2O_3(0001) acquired subsequent to immersion in *CP solution* for 3 h ($h\nu$ = 1486.6 eV, θ_E = 50°). Overview XPS spectra of as-prepared samples (0 h) are also displayed in (a) and (d). For (b), (c), (e), and (f) best fits (light blue markers) to the experimental data (solid black lines) are also shown, achieved with GL (red lines), and Shirley-type (broken grey lines) functions. Peak assignments, as discussed in the text, are indicated.

Figure 6 (a) O 1s core level XPS spectra of rutile-TiO_2(110) acquired from as-prepared sample (0 h), and subsequent to immersion in *CP solution* for 3 h ($h\nu$ = 1486.6 eV, θ_E = 50°). (b) Equivalent data acquired from α-Al_2O_3(0001).

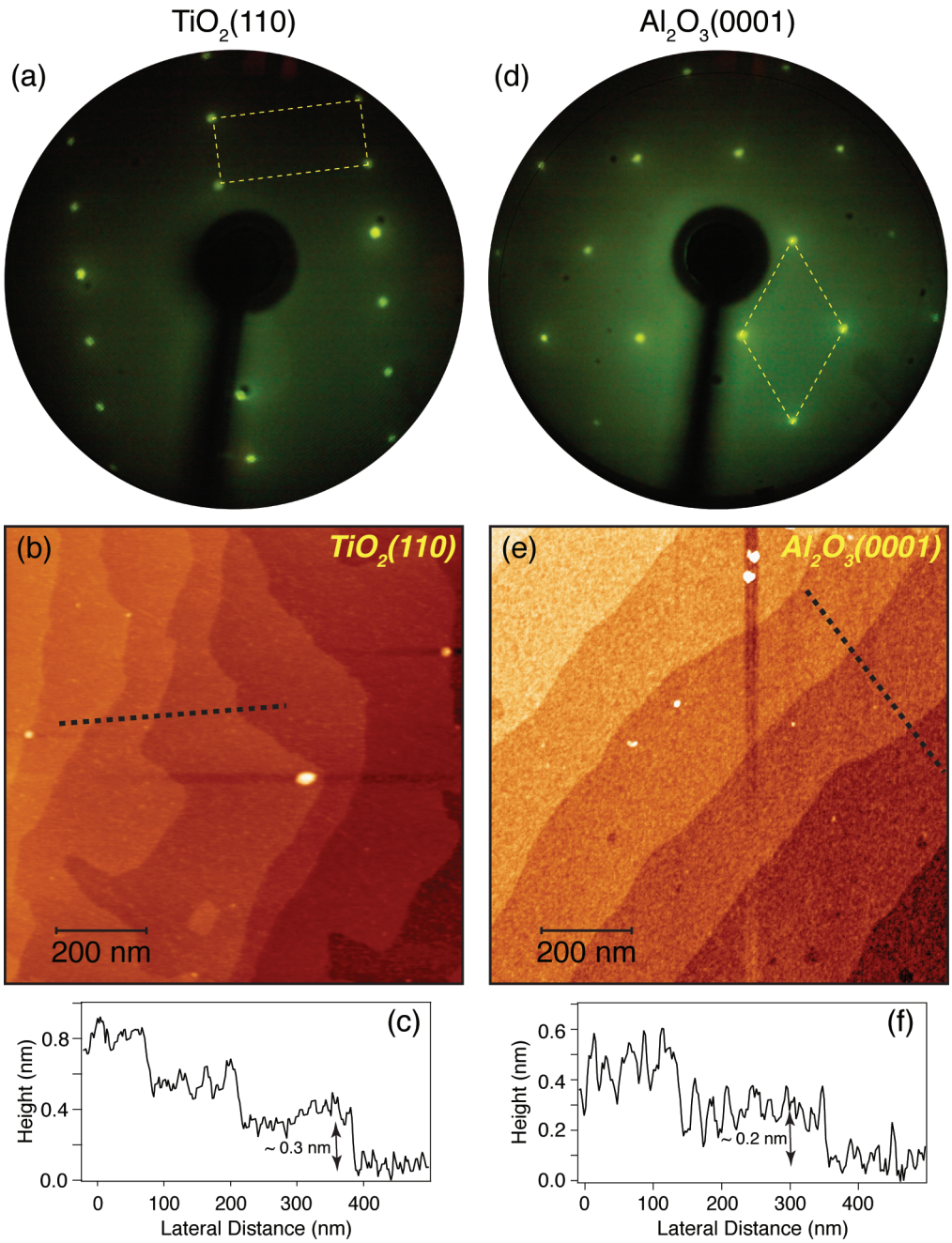
TiO2(110)
Al2O3(0001)
(a)
(d)
(b)
TiO2(110)
200 nm
(e)
Al2O3(0001)
200 nm
(c)
Height (nm)
0.8
0.4
0.0
~ 0.3 nm
0
100
200
300
400
Lateral Distance (nm)
(f)
Height (nm)
0.6
0.4
0.2
0.0
~ 0.2 nm
0
100
200
300
400
Lateral Distance (nm)

Figure 1

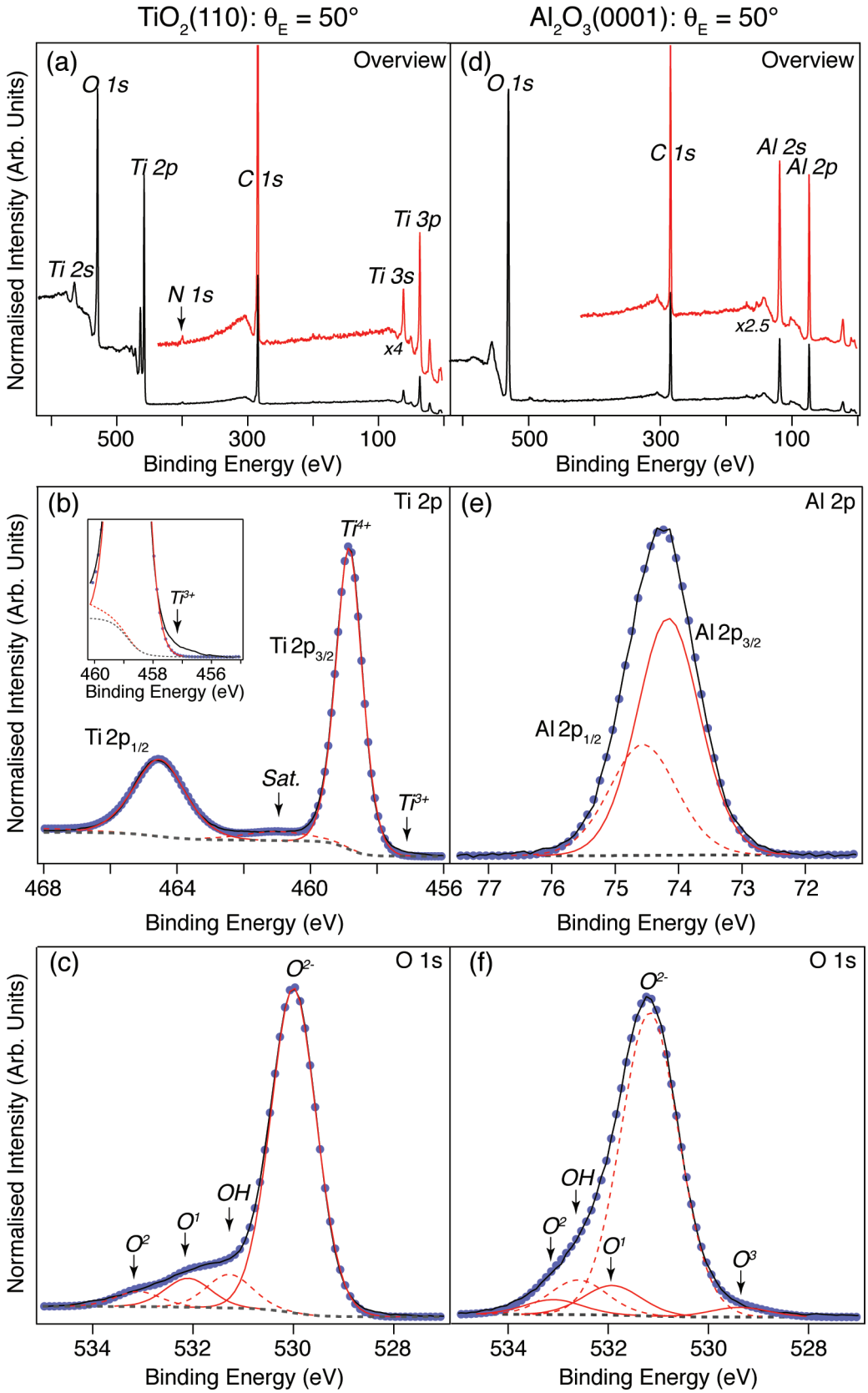
TiO2(110): θE = 50°
Al2O3(0001): θE = 50°
(a)
Overview
O 1s
Ti 2p
C 1s
Ti 3p
Ti 2s
N 1s
Ti 3s
x4
(d)
Overview
O 1s
C 1s
Al 2s
Al 2p
x2.5
Normalised Intensity (Arb. Units)
500
300
100
Binding Energy (eV)
(b)
Ti 2p
Ti4+
Ti3+
Ti 2p3/2
Ti 2p1/2
Sat.
Ti3+
460
458
456
Binding Energy (eV)
(e)
Al 2p
Al 2p3/2
Al 2p1/2
468
464
460
456
77
76
75
74
73
72
(c)
O 1s
O2-
OH
O1
O2
(f)
O 1s
O2-
OH
O2
O1
O3
534
532
530
528

Figure 2

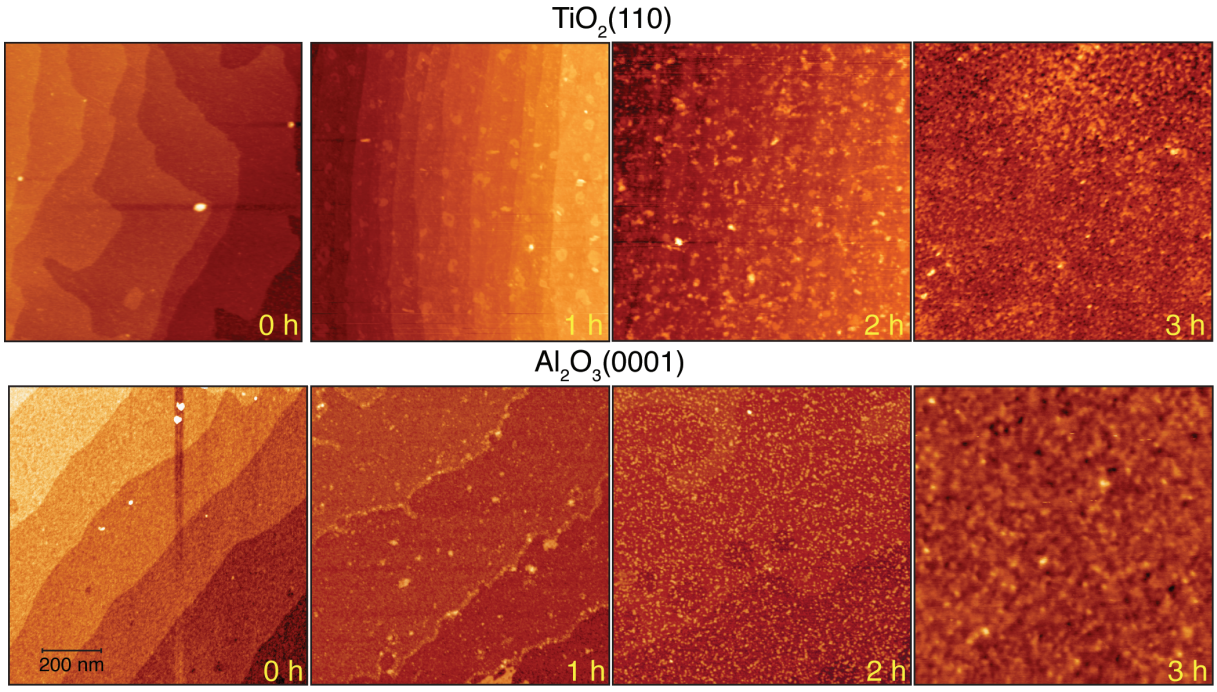

Figure 3

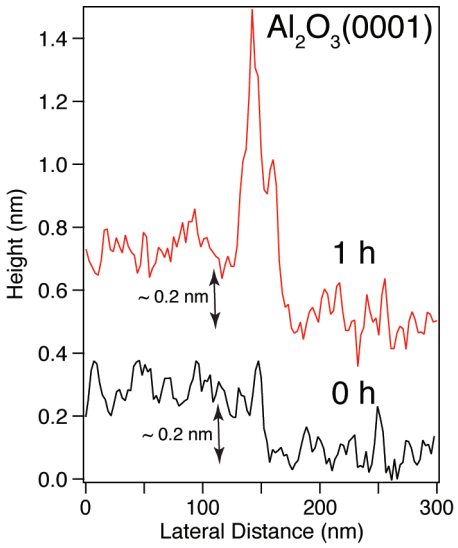
Al2O3(0001)
1 h
0 h
~ 0.2 nm
~ 0.2 nm
Height (nm)
Lateral Distance (nm)
0.0
0.2
0.4
0.6
0.8
1.0
1.2
1.4
0
100
200
300

Figure 4

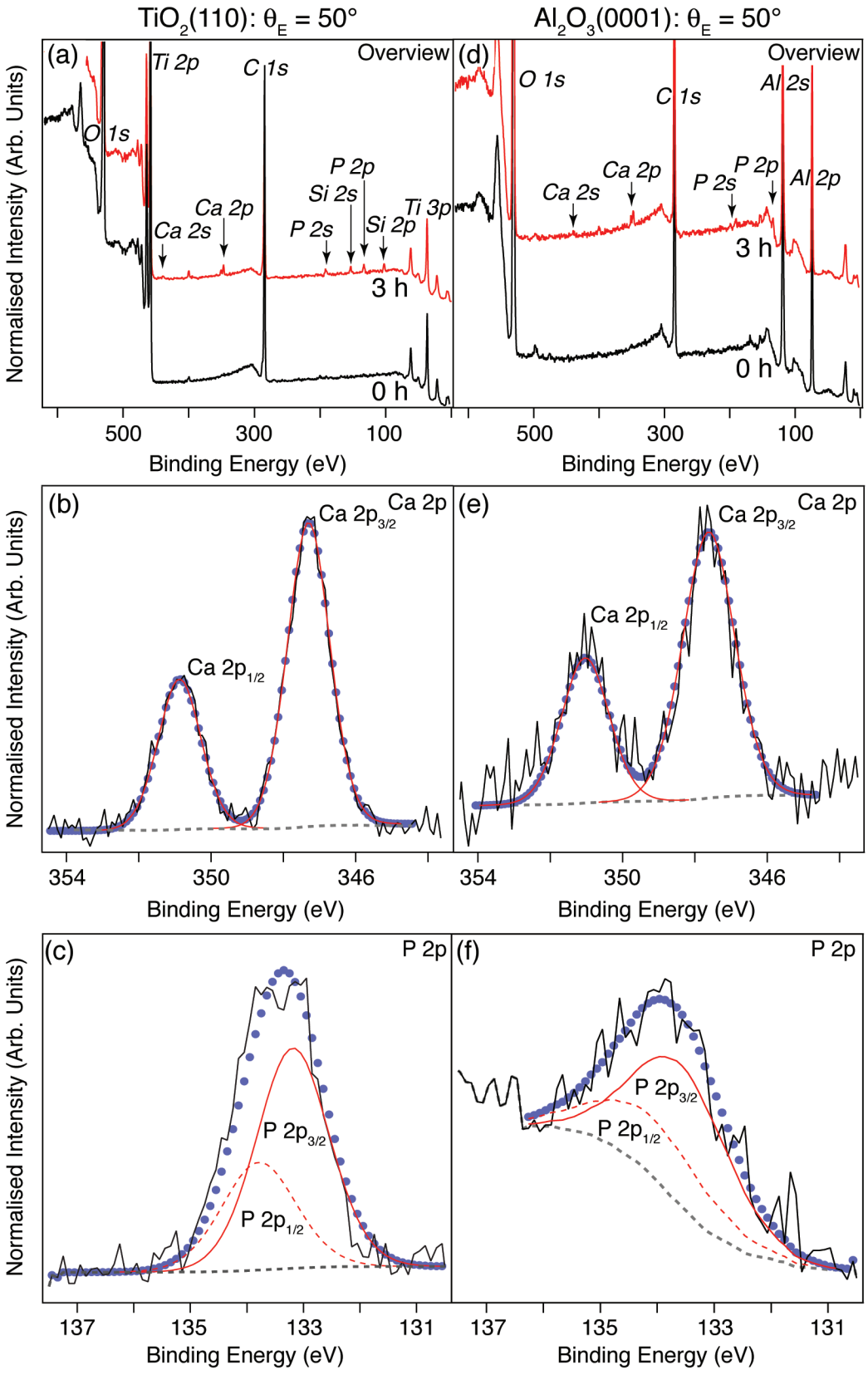
TiO2(110): θE = 50°
Al2O3(0001): θE = 50°
(a)
Overview
Ti 2p
C 1s
O 1s
Ca 2p
Ca 2s
P 2p
Si 2s
P 2s
Si 2p
Ti 3p
3 h
0 h
(d)
Overview
O 1s
C 1s
Al 2s
Ca 2p
Ca 2s
P 2p
P 2s
Al 2p
3 h
0 h
Normalised Intensity (Arb. Units)
Binding Energy (eV)
500
300
100
(b)
Ca 2p
Ca 2p3/2
Ca 2p1/2
(e)
Ca 2p
Ca 2p3/2
Ca 2p1/2
354
350
346
(c)
P 2p
P 2p3/2
P 2p1/2
(f)
P 2p
P 2p3/2
P 2p1/2
137
135
133
131

Figure 5

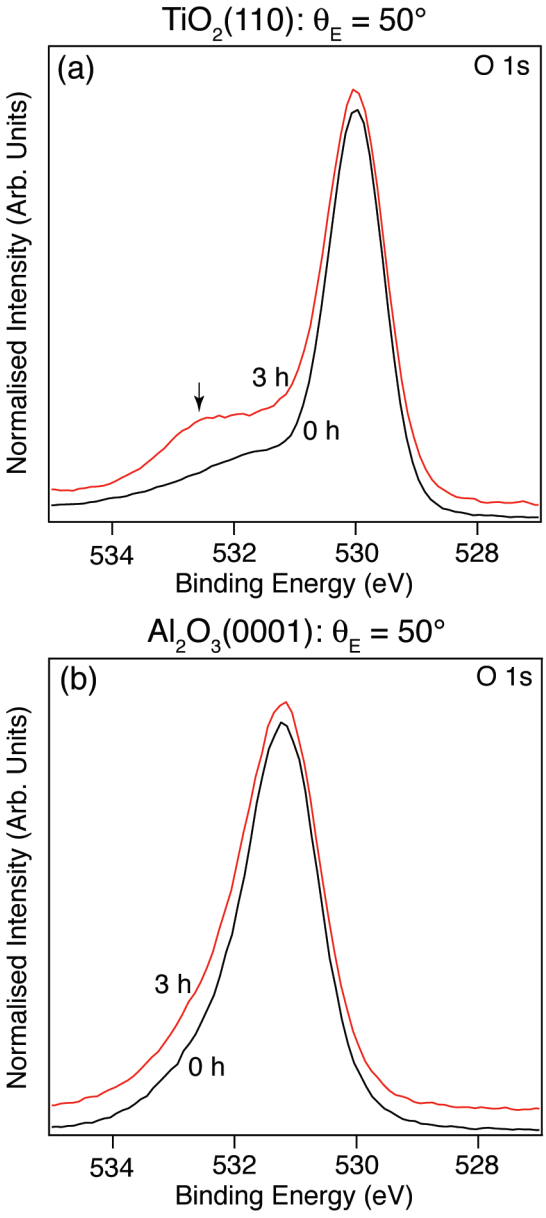
TiO2(110): θE = 50°
(a)
O 1s
3 h
0 h
Normalised Intensity (Arb. Units)
534
532
530
528
Binding Energy (eV)
Al2O3(0001): θE = 50°
(b)
O 1s
3 h
0 h
Normalised Intensity (Arb. Units)
534
532
530
528
Binding Energy (eV)

Figure 6